Clinical Kidney Journal

Clinical Kidney Journal, 2024, vol. 17, no. 12, sfae340

https://doi.org/10.1093/ckj/sfae340
Advance Access Publication Date: 11 November 2024
Original Article

ORIGINAL ARTICLE

Non-invasive assessment of IgA nephropathy severity with [^{18}F]AlF-NOTA-FAPI-04 PET/CT imaging

Hao Wang*, Limeng He*, Lijuan Feng, Weiwei Zhang, Nan Liu and Wei Zhang

Department of Nuclear Medicine, Sichuan Provincial People's Hospital, University of Electronic Science and Technology of China, Chengdu Sichuan, China

*These authors contributed equally to this work and should be considered co-first authors.
Correspondence to: Wei Zhang; E-mail: zhangwscd@uestc.edu.cn, Nan Liu; E-mail: everydayhappy815@163.com

ABSTRACT

Background. Renal biopsy plays a crucial role in diagnosing and assessing the severity of immunoglobulin A nephropathy (IgAN), despite being an invasive procedure with potential risk of failure. Our study focused on evaluating the capability of [^{18}F]AlF-NOTA-FAPI-04 PET/CT in identifying the extent of pathological alterations in IgAN.
Methods. Twenty patients (13 males and 7 females; mean age, 44 ± 16 years) with newly diagnosed primary IgAN and 10 patients (7 males and 3 females; mean age, 51 ± 4 years) without known renal disease underwent [^{18}F]AlF-NOTA-FAPI-04 PET/CT imaging. Kidney tissues from biopsies were stained with various techniques and examined using immunofluorescence. The Oxford classification was used to evaluate pathological indicators. Immunohistochemical staining was conducted to assess α-smooth muscle actin (αSMA) and fibroblast activation protein (FAP) expression. Renal FAPI uptake measured by positron emission tomography/computed tomography (PET/CT) (maximum and mean standardized uptake value, SUV_{max} and SUV_{mean}) was correlated with histological findings.
Results. The renal parenchymal FAPI uptake was significantly higher in IgAN patients compared with control patients ($SUV_{max} = 3.9 \pm 1.3$ vs 1.9 ± 0.4, $SUV_{mean} = 3.6 \pm 1.2$ vs 1.5 ± 0.4; all $P < .001$). We identified a significant difference in renal parenchymal FAPI uptake among the various categories of the Oxford classification. Correlation analysis revealed a positive association between SUV_{max} and interstitial fibrosis and tubular atrophy, as well as tubulointerstitial inflammation scores in scarred cortex and non-scarred cortex ($r = 0.637$, 0.593 and 0.491, all $P < .05$), Similar associations were observed between SUV_{mean} and these scores ($r = 0.641$, 0.592 and 0.479, all $P < .05$). Furthermore, significant positive correlations were observed between SUV_{max} or SUV_{mean} and the staining scores for glomerular αSMA and FAP, as well as for tubulointerstitial αSMA and FAP (all $P < .01$).
Conclusion. [^{18}F]AlF-NOTA-FAPI-04 PET/CT imaging offers IgAN patients a non-invasive and reproducible auxiliary modality to monitor disease progression.

Received: 9.6.2024; Editorial decision: 30.9.2024

GRAPHICAL ABSTRACT

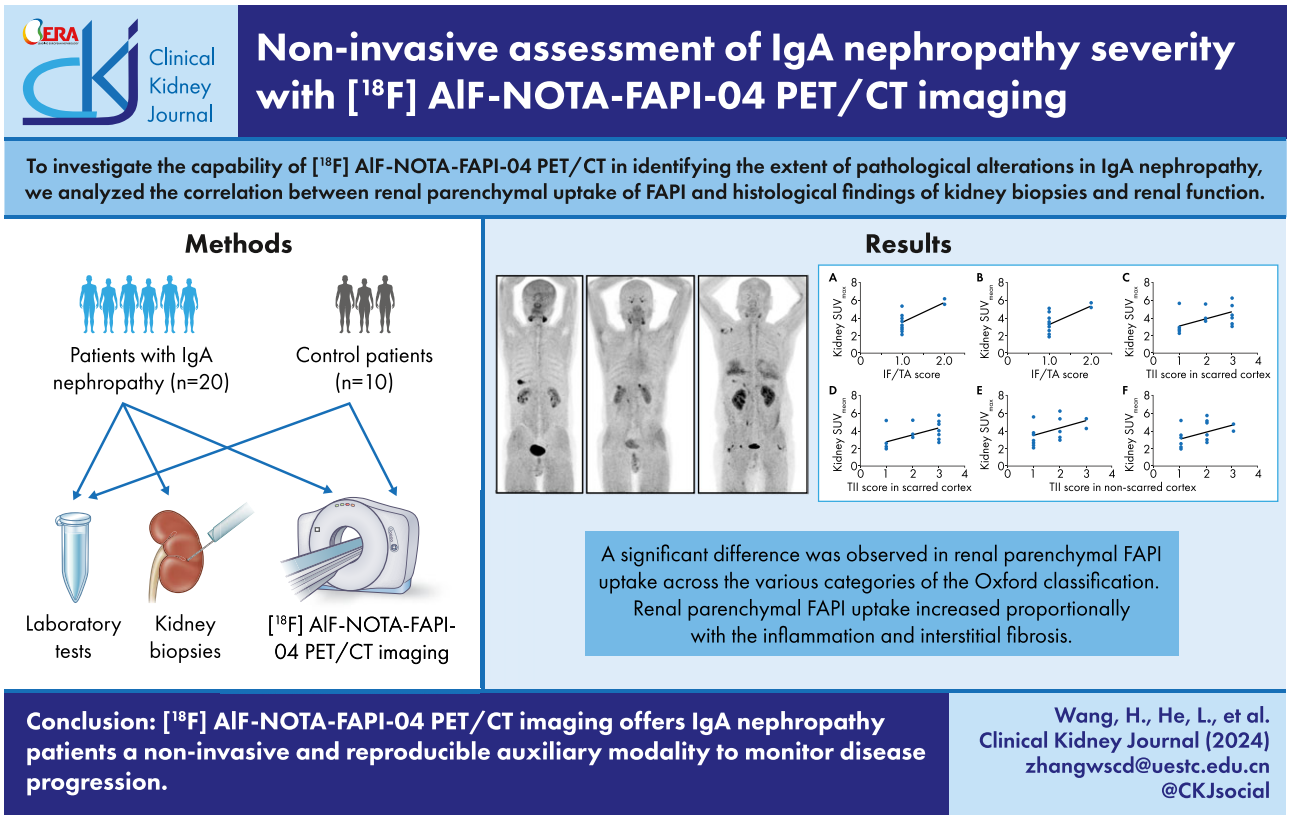

Keywords: [18F]AlF-NOTA-FAPI-04, fibroblast activation protein, IgA nephropathy, interstitial fibrosis, positron emission tomography/computed tomography

KEY LEARNING POINTS

What was known:

- Immunoglobulin A nephropathy (IgAN) is the most common primary glomerulonephritis globally and a major cause of kidney failure.
- Kidney biopsy is crucial for diagnosing IgAN, despite its limitations.
- [18F]AlF-NOTA-FAPI-04 is a novel positron emission tomography (PET) ligand that specifically targets fibroblast activation protein (FAP) expression as a FAP inhibitor (FAPI) and has been demonstrated to have high uptake in fibrotic diseases.

This study adds:

- We provided the first evidence that the uptake of FAPI in the renal parenchyma of IgAN patients correlated with the Oxford classification, as well as interstitial inflammation and fibrosis in the kidneys.
- There were strong associations between FAPI uptake and staining scores for α-smooth muscle actin and FAP, while an inverse relationship was observed with the estimated glomerular filtration rate.

Potential impact:

- Our study suggests that [18F]AlF-NOTA-FAPI-04 PET/computed tomography can serve as a non-invasive method for assessing inflammation and fibrosis, offering valuable insights into the pathological severity in IgAN patients.
- We hope that our findings contribute to the understanding of the potential of this novel molecular imaging technique in evaluating the pathological severity in IgAN.

INTRODUCTION

Immunoglobulin A nephropathy (IgAN) is the most common primary glomerulonephritis globally and a major cause of kidney failure [1]. The pathogenesis of IgAN is complex and uncertain, with a widely recognized four-hit hypothesis [2–5]. In the initiation and advancement of renal dysfunction in IgAN, renal inflammation plays a critical role [6]. Continual inflammation results in advancing fibrosis due to an abundance of fibroblasts and myofibroblasts, along with heightened extracellular matrix synthesis [7]. The extent of interstitial fibrosis and tubular atrophy serves as the most reliable predictor of renal survival [8].

Kidney biopsy is crucial for diagnosing IgAN. Immunofluorescence detects IgA deposits in the glomeruli, while routine histology shows the severity of both active and chronic renal lesions. The spectrum of renal lesions varies significantly, ranging from minor or imperceptible to diffuse proliferative or crescentic [9]. Pathological characteristics offer essential prognostic insights for doctors. Despite progress in medical technology which has improved the safety of kidney biopsies, the procedure is still invasive and cannot be conducted often [10]. The decision to proceed with renal biopsy for cases of simple hematuria or asymptomatic proteinuria is a topic of debate. Factors that may hinder the success of a biopsy include severe coagulation issues, uncontrolled hypertension, pregnancy, anatomical abnormalities and a patient's reluctance to provide informed consent for the procedure [11, 12]. Therefore, there is a critical need to discover a non-invasive tool that can evaluate the severity of nephropathy in IgAN. In recent years, research on non-invasive examinations related to the early stages of IgAN has made remarkable progress, particularly with the development of urine analysis techniques (such as neutrophil gelatinase-associated lipocalin [13], kidney injury molecule-1 [14], *N*-acetyl-β-D-glucosaminidase [15] and urinary proteomics [16]) and imaging examinations [including magnetic resonance imaging (MRI)-blood oxygen level dependent (BOLD) imaging [17], diffusion kurtosis imaging (DKI) [18], renal ultrasonography radiomics [19] and intravoxel incoherent motion diffusion-weighted imaging (IVIM-DWI) [20]]. Consequently, non-invasive examinations have become increasingly viable.

Fibroblast activation protein (FAP), which belongs to the serine protease dipeptidyl peptidase family and is found on the cell surface [21], has been highlighted in recent studies. These studies have demonstrated an increased accumulation of radiopharmaceuticals based on FAP inhibitors (FAPI) in regions exhibiting inflammation and fibrosis, particularly in cancerous tissues [22–25]. Research on the utilization of various radionuclide-labeled FAPI for diagnosing renal diseases is currently gaining momentum. A preclinical investigation revealed that ^{68}Ga-FAPI-04 positron emission tomography/computed tomography (PET/CT) can efficiently detect renal fibrosis in a rapid and non-invasive manner compared with traditional renal biopsy methods [26]. A recent clinical study further supported this by establishing a correlation between the accumulation of ^{68}Ga-FAPI on PET/CT scans and the severity of kidney fibrosis as determined by immunohistopathology [27]. Moreover, a larger-scale clinical study demonstrated that FAPI uptake levels increased as the glomerular filtration rate (GFR) decreased [28].

Recently we have conducted a prospective cohort study to employ [^{18}F]AlF-NOTA-FAPI-04 PET/CT with a high radiolabel yield and specific activity to assess patients with various renal diseases [29]. Our study yielded promising results in assessing tubular injury, with findings showing that the uptake of FAPI in the renal parenchyma was correlated with the severity of renal inflammation and interstitial fibrosis. Furthermore, in this study, we consider whether [^{18}F]AlF-NOTA-FAPI-04 PET/CT could serve as an auxiliary imaging technique for evaluating the pathological severity in IgAN.

MATERIALS AND METHODS

Study design and population

This prospective study involved 20 patients newly diagnosed with primary IgAN following renal biopsy between September 2022 and May 2024. The inclusion criteria required patients to be 18 years of age or older and capable of comprehending and signing an informed consent form. Exclusion criteria included patients with fewer than 10 glomeruli on light microscopy, as well as those with conditions such as allergic purpura, systemic lupus erythematosus, diabetes mellitus, cirrhosis, and individuals who had received treatment with hormones or other immunosuppressants before renal puncture. Additionally, pregnant individuals (or those planning to become pregnant within 6 months) or lactating women were excluded. Patients were also disqualified if they had uncontrolled cardiopulmonary disease or a mental abnormality that would impair their ability to tolerate PET/CT examination. The control group consisted of 10 patients who underwent PET/CT examination for non-kidney diseases during the same period, had normal serum creatinine levels and tested negative for proteinuria. Informed consent, in written form, was received from every participant. This study received approval from the institutional review board (Approval No. 2022–203) and was registered on the Clinical Trial Register (Identifier: NCT05752097). All conducted procedures adhered to ethical standards set by both institutional and national research committees, in alignment with the principles of the 1964 Helsinki Declaration and its later amendments.

Basic demographic details, including age, gender, height, weight and blood pressure, were gathered in the study. Before conducting PET/CT scans, data on blood urea nitrogen (BUN), serum creatinine (Scr), uric acid (UA), hemoglobin (Hb), serum albumin (Alb), total cholesterol, triglycerides and serum immunoglobulin (Ig) levels of IgA, IgG and IgM, as well as complement C3 and C4, were retrieved from the hospital's digital information system. The Scr levels were utilized to compute the estimated GFR (eGFR) following the Chronic Kidney Disease Epidemiology Collaboration formula [30]. Moreover, data on urine erythrocyte count (URBC) and 24-h urine protein (24h-UP) quantification were obtained from patients diagnosed with IgAN.

Synthesis of radiopharmaceuticals

The automatic synthesis procedure of [^{18}F]AlF-NOTA-FAPI-04 was carried out as described previously [31]. The final product [^{18}F]AlF-NOTA-FAPI-04 underwent quality control analysis using instant thin-layer chromatography assessment. The radiochemical purity of the final product exceeded 95%.

PET/CT imaging acquisition

All 30 patients underwent [^{18}F]AlF-NOTA-FAPI-04 PET/CT examinations. Prior to the scans, patients were instructed to consume an adequate amount of water (1 L) and empty their bladders to reduce potential interference from residual radioactive tracers in the kidney. The PET/CT imaging took place approximately 61.2 ± 8.5 min after administering an injection of [^{18}F]AlF-NOTA-FAPI-04 at a dose of 3.70–4.44 MBq (0.10–0.12 mCi)/kg using Flow-

Motion scanning technology. An initial low-dose CT (120 keV; 50 mAs; 1.3 pitch; 3 mm slice thickness; 0.5 s rotation time; estimated radiation dose, 9.0 mGy) was performed for attenuation correction and anatomical localization from the skull to the mid-thigh, followed by a 12-min PET scan using a Biograph mCT Flow 64 PET/CT scanner (Siemens, Germany). PET data were acquired in 3D mode, with patients maintaining normal breathing throughout the image collection. The acquired data were reconstructed using the ordered subset expectation maximization method with 2 iterations and 21 subsets. The collection of study-specific parameters was conducted using the dedicated imaging software Syngo.via (Version VB 40, Siemens Healthineers). Attenuation-corrected PET images, CT images and fused PET/CT images were viewed and analyzed as coronal, sagittal and cross-sectional layers.

Imaging analysis

The PET/CT images underwent independent evaluation by two nuclear medicine specialists, each boasting over 5 years of PET/CT interpretation experience, in a randomized sequence. The clinicians were blinded to the clinical data, and an image interpretation consensus was achieved. Both visual and quantitative assessments were performed. For visual analysis, a three-tier grading scale was used: mild uptake, corresponding to uptake comparable to or slightly exceeding that of the blood pool; moderate uptake, equivalent to two to three times that of the blood pool; and intense uptake, indicating significantly higher uptake than that of the blood pool. Quantitative analysis required the calculation of the maximum standardized uptake value (SUV_{max}) and the mean standardized uptake value (SUV_{mean}), both normalized to body weight. Renal tracer uptake was quantified by either SUV_{max} or SUV_{mean} at specific sites within the renal parenchyma (superior, middle and inferior renal cortex), as previously described [28]. The renal parenchyma SUV_{max} or SUV_{mean} was then determined by averaging the SUV_{max} or SUV_{mean} values across these three specified locations in the renal parenchyma.

Pathohistological examinations

Individuals suffering from renal illness received a renal biopsy post-PET/CT examination within a 7-day timeframe. The renal tissues procured from said biopsies were preserved in formalin, encased in paraffin, and subsequently sliced into sections measuring 2 μm in thickness. Following this, these sections were dyed with hematoxylin and eosin, periodic acid–Schiff, Masson trichome and periodic acid–silver methenamine under a light microscope, and subsequently examined through immunofluorescence techniques.

The number of glomeruli was recorded, and the Oxford classification was employed to assess the rating for each pathological indicator [32]. Mesangial hypercellularity was separated into <50% (M0) and >50% (M1). Endocapillary hypercellularity was characterized as either lacking (E0) or present (E1). Segmental glomerulosclerosis was categorized as either not present (S0) or present (S1). Tubular atrophy/interstitial fibrosis were categorized as ≤25% (T0), 26% to 50% (T1) and >50% (T2). Formation of cellular/fibrocellular crescents was classified as not present (C0), 1% to 25% (C1) and >25% (C2).

A revised scoring system [33] was utilized to evaluate the severity of interstitial fibrosis and tubular atrophy (IF/TA) in IgAN patients, taking into account the mild level of inflammation and fibrosis. Lesions were assessed based on Masson trichrome staining, with a scale from 1 to 3 indicating the extent of IF/TA (1 = ≤25%; 2 = 26–50%; 3 = >50%). Tubulointerstitial inflammation (TII) in scarred and non-scarred cortex were also rated separately on a scale of 1 to 3, reflecting the level of interstitial inflammatory infiltrate seen in tissue samples (1 = <5%, 2 = 5–25%, 3 = >25%).

Immunohistochemical analysis was carried out to assess the levels of α-smooth muscle actin (αSMA) and FAP using antibodies against αSMA (diluted 1:200, M50132; Zhengneng, Chengdu, China) and FAP-alpha (diluted 1:1000, ab53066; Abcam, Cambridge, MA, USA) respectively. Cells showing positive staining for αSMA or FAP were determined by the presence of brown-to-yellow granules or aggregates following respective staining under light microscopy at 200× magnification. The intensity of staining and the proportion of positively stained cells were both evaluated. Staining intensity was graded on a range from 0 to 3 (0 = not visible; 1 = weak; 2 = moderate; 3 = strong). The extent of positive staining was rated based on the percentage of positive cells compared with all cells in the field of view, using a scale from 0 to 4 (0 = none, 1 = <25%, 2 = 25 to <50%, 3 = 50% to ≤75%, 4 = >75%). An overall glomerular or tubulointerstitial score for αSMA or FAP was determined by multiplying the staining intensity by the percentage of positive cells.

Histopathological sections were evaluated by two experienced nephropathologists. Results were based on the average values from ten fields of view, with any discrepancies resolved through consensus.

Statistical analysis

Statistical analysis was carried out utilizing SPSS version 22.0 (SPSS Inc., Chicago, IL, USA). The normality of the quantitative variable was assessed. Continuous variables were depicted as mean with standard deviation or as median accompanied by the relevant range. Inter-group comparisons of independent samples were performed using the Student's *t*-test for data with normal distribution and Wilcoxon test for skewed data (Shapiro–Wilk test for normality). Comparisons of paired samples between groups were conducted using a paired *t*-test for normally distributed data and the paired samples Wilcoxon test for skewed data. Categorical data were shown as proportions or percentages and examined with the Chi-square test. Correlation analyses were executed using either the Pearson correlation coefficients for normally distributed data or the Spearman rank correlation coefficients for skewed data. A *P*-value of <.05 in a two-sided test was considered statistically significant.

RESULTS

Population study characteristics

A total of 20 subjects diagnosed with primary IgAN were enrolled in Group A, containing 13 men and 7 women with an average age of 44 ± 16 years. The illness duration varied from 4 days to 5 years. Clinical features were described in Supplementary data, Table S1. Group B acted as the control cohort, comprising 10 participants without evidence of kidney disease, with 7 males and 3 females and an average age of 51 ± 4 years. No significant variations in gender, age, body mass index or blood pressure were detected between the two groups. Additionally, the levels of BUN, Scr and serum IgA in patients from Group A were significantly higher than those in Group B, whereas eGFR, albumin and serum C3 levels were significantly lower in Group A compared with

Table 1: Clinical characteristics of enrolled patients ($n = 30$).

Characteristic	Group A ($n = 20$)	Group B ($n = 10$)	P-value
Age (years)	44 ± 16	51 ± 4	.147
Male gender, n (%)	13 (65)	7 (70)	1.000
BMI (kg/m^2)	22.3 ± 2.5	22.8 ± 2.1	.575
SBP (mmHg)	138.3 ± 9.3	137.6 ± 7.8	.840
DBP (mmHg)	81.5 ± 6.5	80.8 ± 5.3	.770
BUN (mmol/L)	9.9 ± 4.7	5.1 ± 1.1	.004**
Scr (μmol/L)	148.9 ± 86.4	66.9 ± 15.9	.006**
UA (μmol/L)	419.8 ± 96.3	358.1 ± 55.6	.073
eGFR (mL/min/1.73 m^2)	73.4 ± 36.5	101.0 ± 15.5	.031*
Hb (g/L)	118.0 ± 23.7	127.7 ± 23.4	.298
Alb (g/L)	34.3 ± 5.2	38.7 ± 4.9	.034*
TC (mmol/L)	4.39 ± 0.58	4.41 ± 0.67	.957
TG (mmol/L)	1.4 ± 0.5	1.5 ± 0.4	.771
Serum IgA (g/L)	2.9 ± 0.7	1.8 ± 0.5	.001**
Serum IgG (g/L)	11.9 ± 2.3	12.1 ± 1.9	.779
Serum IgM (g/L)	0.9 ± 0.3	1.0 ± 0.4	.846
Serum C3 (g/L)	0.9 ± 0.2	1.1 ± 0.3	.011*
Serum C4 (g/L)	0.3 ± 0.1	0.3 ± 0.1	.963

Data are presented as mean ± SD or n (%).
BMI, body mass index; SBP, systolic blood pressure; DBP, diastolic blood pressure; TC, total cholesterol; TG, triglycerides.
**$P < .01$, *$P < .05$.

Group B. Specific details on the population study characteristics are provided in Table 1.

Performance of [^{18}F]AlF-NOTA-FAPI-04 PET/CT imaging in the study population

Upon initial inspection of the FAPI imaging, it was noted that every single one of the 20 patients diagnosed with IgAN exhibited varying levels of renal parenchymal uptake. Specifically, seven individuals displayed mild uptake, seven showed moderate uptake and six demonstrated intense uptake. Typical images are illustrated in Figs 1 –3. Analysis of the SUV_{max} and SUV_{mean} values of the renal parenchyma revealed a significant inverse relationship with eGFR levels (correlation coefficient $r = –0.766$ and –0.757, all statistical significance levels at $P < .001$) (refer to Fig. 4). Conversely, all 10 participants in the comparison group displayed mild renal parenchymal uptake based on visual assessment. The SUV_{max} and SUV_{mean} values in Group A were markedly higher than those in Group B (3.9 ± 1.3 compared with 1.9 ± 0.4 and 3.6 ± 1.2 compared with 1.5 ± 0.4, respectively; $t = 6.380$ and 6.863, all $P < .001$).

In the PET/CT scans of the patient 12, in addition to the widespread FAPI uptake in the renal parenchyma, we also observed a heightened diffuse and irregular FAPI uptake in the lower lobes of both lungs, along with increased FAPI uptake in the joints of both shoulders and hips (see Supplementary data, Fig. S1).

Association of clinical characteristics with Oxford classification and renal parenchymal FAPI uptake

Significant differences were observed between the Oxford classification M0 group and the M1 group in terms of BUN, Scr, UA, eGFR, hemoglobin (Hb), Alb and serum C3 ($P < .05$). Additionally, significant differences were found between the E0 group and the E1 group solely in Hb levels ($P < .01$). The S0 group and the S1 group exhibited significant differences in BUN, Scr, UA, eGFR, albumin (Alb), serum IgA and 24h-UP ($P < .05$). Furthermore, significant differences in UA, eGFR, Alb, serum IgA and 24h-UP were noted between the T0 group and the T1 group ($P < 0.05$). Lastly, a significant difference in serum C4 was identified between the C0 group and the C1 group ($P < .05$). For further details, please refer to Supplementary data, Table S2.

Table 2 illustrates the relationship between renal parenchymal FAPI uptake, including SUV_{max} and SUV_{mean}, and various clinical characteristics in Group A. Both SUV_{max} and SUV_{mean} demonstrated positive correlations with BUN, Scr, UA, IgA and 24h-UP ($P < .05$), while exhibiting negative correlations with eGFR, Hb and Alb ($P < .01$).

Association of renal parenchymal FAPI uptake with Oxford classification and severities of renal interstitial inflammation and fibrosis

There were significant differences in SUV_{max} and SUV_{mean} between the Oxford classification M0 and M1 groups ($P < .05$). Additionally, significant differences were observed between the S0 and S1 groups, as well as between the T0 and T1 groups ($P < .01$). However, no significant differences were found between the E0 and E1 groups or the C0 and C1 groups ($P > .05$) (Table 3).

The correlation analysis revealed a positive relationship between the SUV_{max} and SUV_{mean} of the renal parenchyma and the IF/TA score ($r = 0.637$, 0.641, $P = .003$ and .002, respectively) (Fig. 5A and B, Supplementary data, Table S3). Similarly, there was a positive correlation observed between the SUV_{max} or SUV_{mean} of the renal parenchyma and the TII score in scarred cortex and non-scarred cortex ($r = 0.593$, 0.491, 0.592, 0.479, $P = .006$, .028, .006 and .033, respectively) (Fig. 5C–F, Supplementary data, Table S3). Following subsequent analysis, it was found that the TII score in the scarred cortex was significantly higher than that in the non-scarred cortex ($Z = 3.162$, $P = .002$). Participants exhibiting mild renal interstitial inflammation in the scarred cortex (TII score = 1) demonstrated notably lower SUV_{max} and SUV_{mean} values compared with those with moderate or severe renal interstitial inflammation in the scarred cortex (2.9 ± 1.2 vs 4.4 ± 1.0 and 2.7 ± 1.1 vs 4.0 ± 1.0, respectively; $t = –2.834$ and –2.831, both $P = .011$) (Fig. 6A and B). Similarly, individuals with mild renal interstitial inflammation in the non-scarred cortex (TII score = 1) showed significantly lower SUV_{max} and SUV_{mean} values in relation to participants with moderate or severe renal interstitial inflammation in the non-scarred cortex (TII score ≥2) (3.4 ± 1.2 vs 4.5 ± 1.1 and 3.1 ± 1.1 vs 4.2 ± 1.0, respectively; $t = –2.157$ and –2.202, $P = .045$ and .041) (Fig. 6C and D). Moreover, the analysis of interstitial fibrosis indicated a comparable trend, with lower levels of SUV_{max} and SUV_{mean} observed in subjects with mild interstitial fibrosis and tubular atrophy (IF/TA score = 1) as opposed to those with moderate or severe interstitial fibrosis and tubular atrophy (IF/TA score ≥2) (3.6 ± 1.1 vs 5.8 ± 0.4 and 3.2 ± 1.0 vs 5.4 ± 0.3, respectively; $t = –3.509$ and –3.543, $P = .003$ and .002) (Fig. 6E and F).

Association between the renal parenchymal FAPI uptake and immunohistochemical staining of FAP and αSMA

The results of the correlation analysis indicated a significant positive correlation between the SUV_{max} of the renal parenchyma and the staining scores for glomerular αSMA and

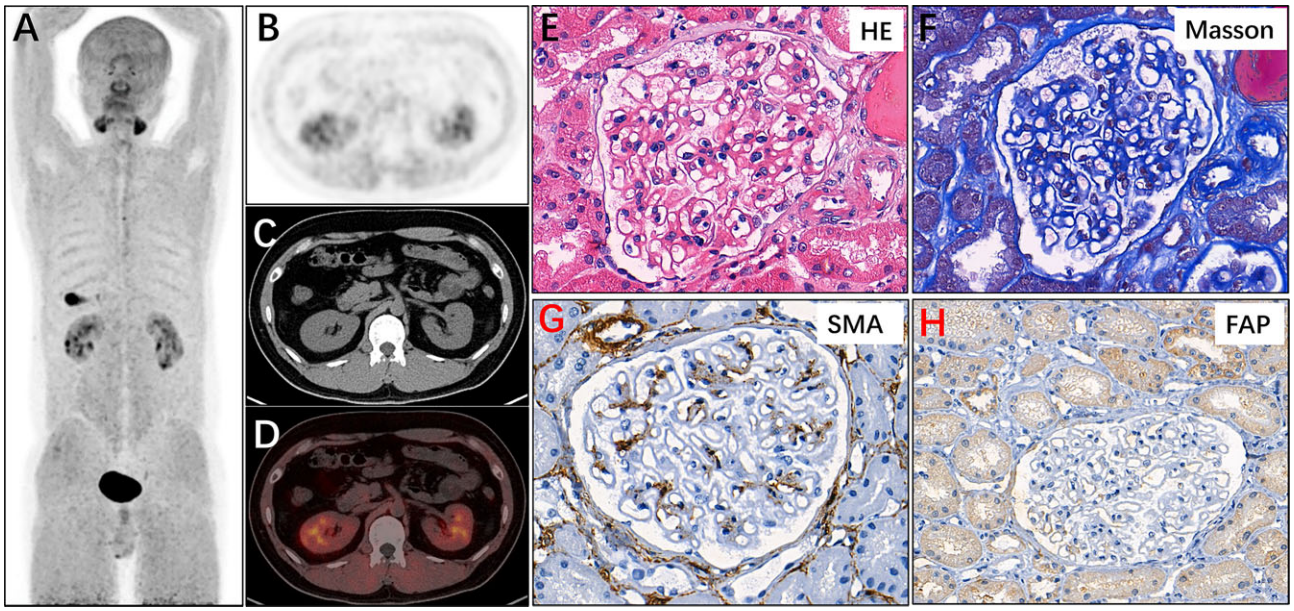

Figure 1: The renal parenchymal FAPI uptake and histological observations in patient 3 exhibiting mild uptake. A 26-year-old male presented with foamy urine for 1 week. (**A**) The maximum intensity projection (MIP) image of the whole-body [^{18}F]AlF-NOTA-FAPI-04 PET/CT scan showed varied uptake of the radiotracer in both kidneys. (**B–D**) The cross-sectional images displayed slight radiotracer uptake in the renal parenchyma, with SUV_{max} and SUV_{mean} values of 2.88 and 2.54, respectively. Renal pathological examination confirmed a diagnosis of IgAN with normal glomeruli. The glomeruli exhibit delicate, ribbon-like glomerular basement membranes with open capillary loops. There is no mesangial hypercellularity, endocapillary hypercellularity, sclerosis of the capillary tuft or crescent formation (M0 E0 S0 T0 C0, TII score in scarred cortex = 1, TII score in non-scarred cortex = 1, IF/TA score = 1) (**E**, **F**). Immunochemical analysis indicated mild expression of αSMA and FAP in the mesangial region of the glomeruli, renal interstitium and tubules (glomerular αSMA staining score = 4, tubulointerstitial αSMA staining score = 4, glomerular FAP staining score = 1, tubulointerstitial FAP staining score = 2) (**G**, **H**).

FAP ($r = 0.667$ and 0.604, both $P < .01$), as well as for tubulointerstitial αSMA and FAP ($r = 0.781$ and 0.758, both $P < .001$) (see Fig. 7A–D, and Supplementary data, Table S4). Additionally, a significant positive correlation was observed between the SUV_{mean} of the renal parenchyma and the staining scores for glomerular αSMA and FAP ($r = 0.622$ and 0.578, both $P < .01$), and for tubulointerstitial αSMA and FAP ($r = 0.755$ and 0.779, both $P < .001$) (refer to Fig. 7E–H, Supplementary data, Table S4).

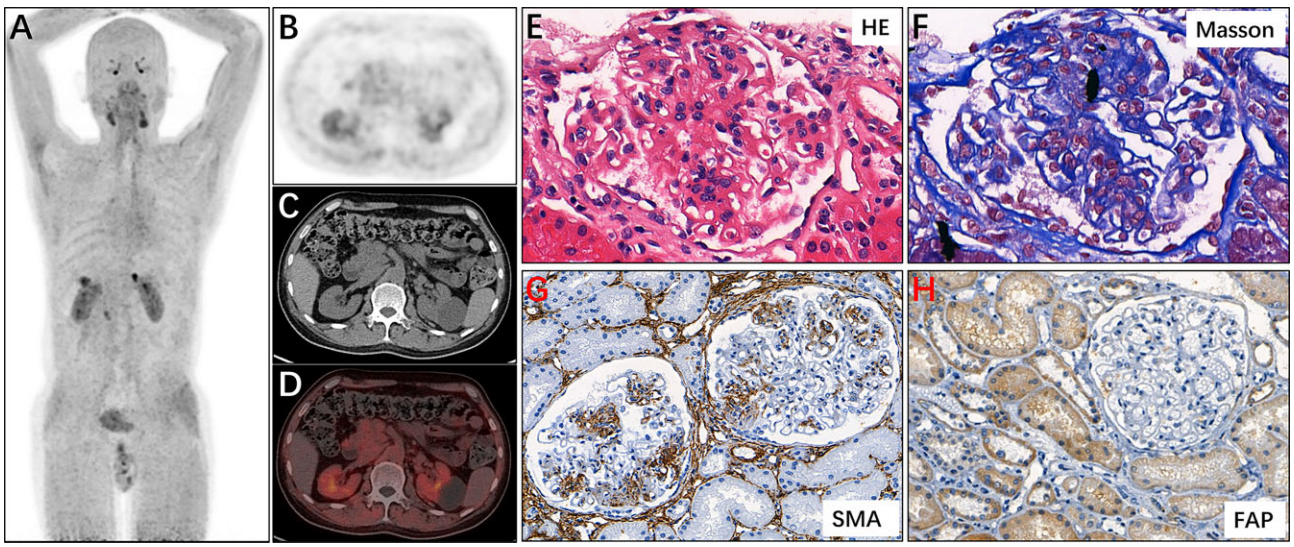

Figure 2: The renal parenchymal FAPI uptake and histological observations in patient 2 exhibiting moderate uptake. A 54-year-old male presented with elevated creatinine levels persisting for 3 years. (**A**) The maximum intensity projection (MIP) image from whole-body [^{18}F]AlF-NOTA-FAPI-04 PET/CT showed diffuse radiotracer uptake in both kidneys. (**B–D**) Cross-sectional images revealed moderate radiotracer uptake in the renal parenchyma, with SUV_{max} and SUV_{mean} values of 3.62 and 3.23, respectively. Subsequent renal pathology confirmed IgAN with mesangial hypercellularity and segmental sclerosis (M1 E0 S1 T0 C0, TII in scarred cortex score = 2, TII score in non-scarred cortex = 1, IF/TA score = 2) (**E**, **F**). Immunohistochemical analysis showed moderate expression of αSMA and FAP in the mesangial region of the glomeruli, renal interstitium, and tubules (glomerular αSMA staining score = 6, tubulointerstitial αSMA staining score = 9, glomerular FAP staining score = 2, tubulointerstitial FAP staining score = 3) (**G**, **H**).

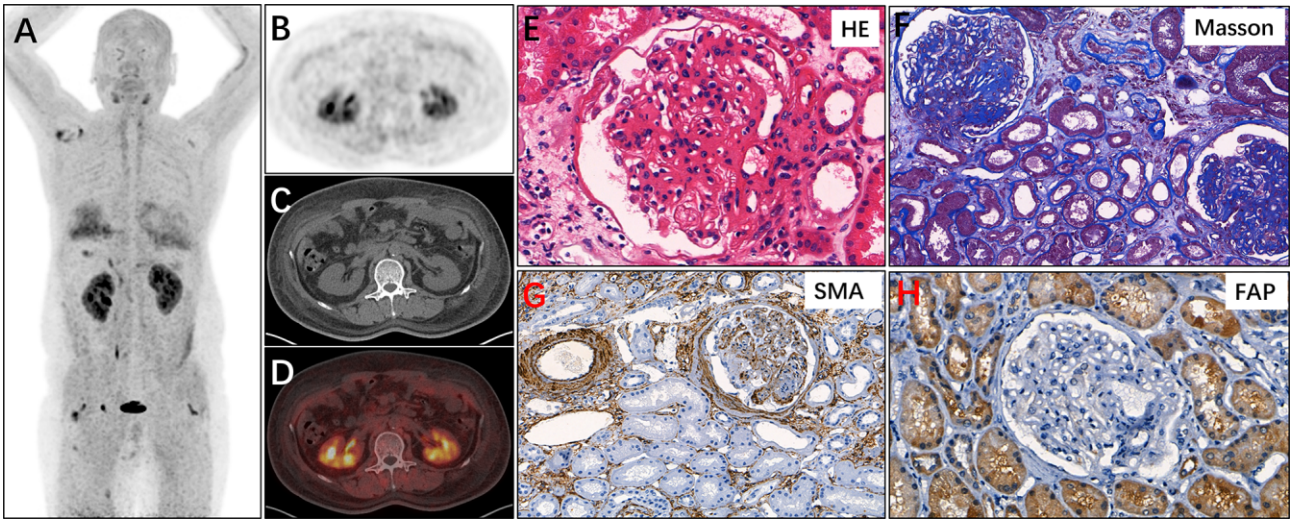

Figure 3: The renal parenchymal FAPI uptake and histological observations in patient 12 exhibiting intense uptake. A 60-year-old male presented with facial and lower limb edema for 2 months. (**A**) The maximum intensity projection (MIP) image obtained from whole-body [^{18}F]AlF-NOTA-FAPI-04 PET/CT showed widespread uptake of radiotracer in both kidneys. (**B–D**) The cross-sectional images displayed high radiotracer uptake in the renal parenchyma, with SUV_{max} and SUV_{mean} values of 5.36 and 4.99, respectively. Pathological examination confirmed a diagnosis of IgAN with mesangial hypercellularity, segmental sclerosis and fibrocellular crescent (M1 E0 S1 T0 C1, TII in scarred cortex score = 3, TII score in non-scarred cortex = 2, IF/TA score = 2) (**E, F**). Immunohistochemical analysis indicated significant expression of αSMA and FAP in the mesangial region of the glomeruli, renal interstitium and tubules (glomerular αSMA staining score = 9, tubulointerstitial αSMA staining score = 9, glomerular FAP staining score = 2, tubulointerstitial FAP staining score = 6) (**G, H**).

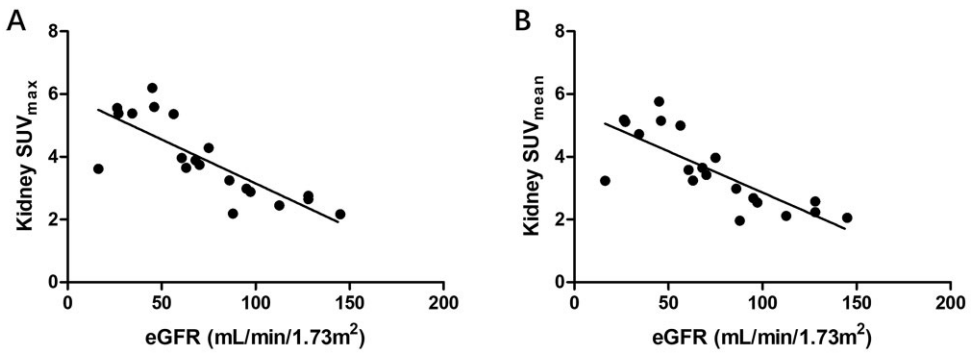

Figure 4: Correlation of the renal parenchymal FAPI uptake with eGFR levels. (**A**) The SUV_{max} exhibited a significant negative correlation with the eGFR levels ($r = -0.766$, $P < .001$). (**B**) The SUV_{mean} exhibited a significant negative correlation with the eGFR levels ($r = -0.757$, $P < .001$).

DISCUSSION

The research utilized [^{18}F]AlF-NOTA-FAPI-04 PET/CT imaging to evaluate individuals with IgAN, demonstrating encouraging prospects for evaluating renal pathological severity. Notably, FAPI uptake in the renal parenchyma was found to increase with the Oxford classification, as well as with the extent of interstitial inflammation and fibrosis in the kidneys. Additionally, strong correlations were identified between FAPI uptake and staining scores for αSMA and FAP, while an inverse relationship was observed with the eGFR. Our research represents the first application of [^{18}F]AlF-NOTA-FAPI-04 PET/CT in patients with IgAN, indicating that [^{18}F]AlF-NOTA-FAPI-04 PET/CT imaging may serve as a valuable non-invasive tool for the long-term evaluation of renal pathological injury in this patient population.

IgAN is a complex disease with diverse clinical and histopathological characteristics [34]. Accurately predicting renal prognoses based on clinical and pathological findings is crucial for determining appropriate preventive treatments. In clinical practice, the Oxford classification is currently the most commonly utilized pathological classification system for IgAN, with an update released in 2017 [32, 35]. This classification identifies five key histopathological features that are crucial for predicting IgAN prognosis. Due to the invasive nature of renal biopsy and the associated risk of complications like bleeding, patients with absolute contraindications are unable to undergo this procedure [36]. Hence, there is a need to investigate non-invasive and convenient imaging techniques for assessing renal function and pathology in IgAN patients.

Blood oxygen level dependent (BOLD)-MRI is currently the preferred method for noninvasively examining kidney tissue, specifically imaging internal oxygen content and blood oxygen saturation. Khatir *et al.* [17] demonstrated that MRI-based measurements of renal arterial blood flow (RABF) and cortical BOLD are reproducible in both healthy controls and patients with chronic kidney disease (CKD), while medullary R_2^* values

Table 2: Correlation between the renal parenchymal FAPI uptake and clinical characteristics in Group A ($n = 20$).

Clinical characteristics	SUV_{max}	SUV_{mean}
BUN (mmol/L)		
R-value	0.486	0.483
P-value	.030*	.031*
Scr (μmol/L)		
R-value	0.660	0.661
P-value	.002**	.002**
UA (μmol/L)		
R-value	0.786	0.785
P-value	<.001**	<.001**
eGFR (mL/min/1.73 m^2)		
R-value	–0.803	–0.791
P-value	<.001**	<.001**
Hb (g/L)		
R-value	–0.577	–0.568
P-value	.008**	.009**
Alb (g/L)		
R-value	–0.848	–0.836
P-value	<.001**	<.001**
TC (mmol/L)		
R-value	0.266	0.245
P-value	.257	.298
TG (mmol/L)		
R-value	0.272	0.259
P-value	.245	.271
IgA (g/L)		
R-value	0.680	0.668
P-value	.001**	.001**
IgG (g/L)		
R-value	0.039	0.011
P-value	.871	.963
IgM (g/L)		
R-value	–0.419	–0.406
P-value	.066	.076
C3 (g/L)		
R-value	–0.400	–0.416
P-value	.081	.068
C4 (g/L)		
R-value	0.182	0.199
P-value	.441	.401
URBC (pieces/ul)		
R-value	0.063	–0.065
P-value	.791	.786
24h-UP (g/24 h)		
R-value	0.821	0.816
P-value	<.001**	<.001**

TC, total cholesterol; TG, triglycerides; URBC, urine erythrocyte count.
**P < .01, *P < .05.

Table 3: FAPI uptake in renal parenchyma of patients in Group A with different Oxford classification ($n = 20$).

Oxford classification	SUV_{max}	SUV_{mean}
M0	3.4 ± 1.2	3.0 ± 1.1
M1	4.6 ± 1.0	4.2 ± 0.9
P-value	.032*	.033*
E0	3.9 ± 1.4	3.6 ± 1.3
E1	3.7 ± 1.1	3.4 ± 0.9
P-value	.742	.675
S0	3.2 ± 0.9	2.9 ± 0.8
S1	4.7 ± 1.2	4.3 ± 1.2
P-value	.006**	.005**
T0	3.5 ± 1.0	3.1 ± 1.0
T1	5.7 ± 0.4	5.2 ± 0.4
P-value	<.001**	.001**
C0	3.7 ± 1.2	3.4 ± 1.1
C1	5.4 ± 0.1	5.1 ± 0.1
P-value	.085	.064

**P < .01, *P < .05.

exhibited intermediate reproducibility in patients. Furthermore, they found that inhalation of pure oxygen increases medullary R_2*. This imaging technique compensates for the limitations of laboratory biochemical examinations and other auxiliary methods; however, it cannot quantitatively detect the partial pressure of oxygen. Additionally, steps need to be taken to enhance the accuracy of R_2* values. Liu *et al.* [18] evaluated renal fibrosis in IgAN using diffusion kurtosis imaging (DKI) and proposed that the non-Gaussian DKI model could serve as a potential method for assessing renal fibrosis in CKD patients with IgAN. This method also offers additional insights compared with conventional DWI. However, further studies are required to validate the feasibility of this method for longitudinal monitoring in patients with IgAN. The potential use of renal ultrasonography radiomics features in classifying glomerulopathy histologically was examined by Zhang *et al.* [19]. Their study revealed that the quantitative radiomics imaging characteristics obtained from digital renal ultrasound can effectively differentiate IgAN from minimal change nephropathy. This analysis of radiomics serves as a non-invasive approach, offering advantages for the histological classification of glomerulopathy. Mao and colleagues [20] explored the clinical significance of intravoxel incoherent motion diffusion-weighted imaging (IVIM-DWI) for assessing renal pathological damage in individuals suffering from IgAN. They evaluated this approach against a mono-exponential model and revealed that IVIM-DWI shows enhanced diagnostic capability compared with the mono-exponential model for evaluating renal pathological injury in patients with IgAN. The aforementioned imaging detection methods offer innovative approaches for the early non-invasive diagnosis of IgAN. Nevertheless, these assessment techniques currently demonstrate inadequate sensitivity and specificity when utilized as standalone diagnostic tools.

The kidney is a complex organ made up of various types of cells that form the glomeruli, tubules, interstitium and capillaries. Glomerular fibrosis can result from glomerular IgA deposition, while tubulointerstitial fibrosis may be triggered by infections or proteinuria [37]. The degree of interstitial fibrosis and tubular atrophy has proven to be the strongest predictor of renal survival [38], so early and accurate assessment of the degree of fibrosis in the kidney is critical to improving the effectiveness of current anti-fibrotic treatments. Our research findings revealed a significant correlation between the level of FAPI absorption in kidney tissue and the scores for IF/TA. Specifically, subjects with moderate or severe IF/TA (scores $\geq$2) exhibited higher levels of SUV_{max} and SUV_{mean} compared with those with mild IF/TA (score = 1). Subsequent immunohistochemical analysis demonstrated an increase expression of αSMA in both glomerular and tubulointerstitial regions, indicative of a higher number of myofibroblasts, in renal tissue with elevated FAPI uptake. The expression of αSMA was primarily observed in the mesangium of glomeruli and the interstitial tissue of the kidney. These results provided further evidence supporting the important role

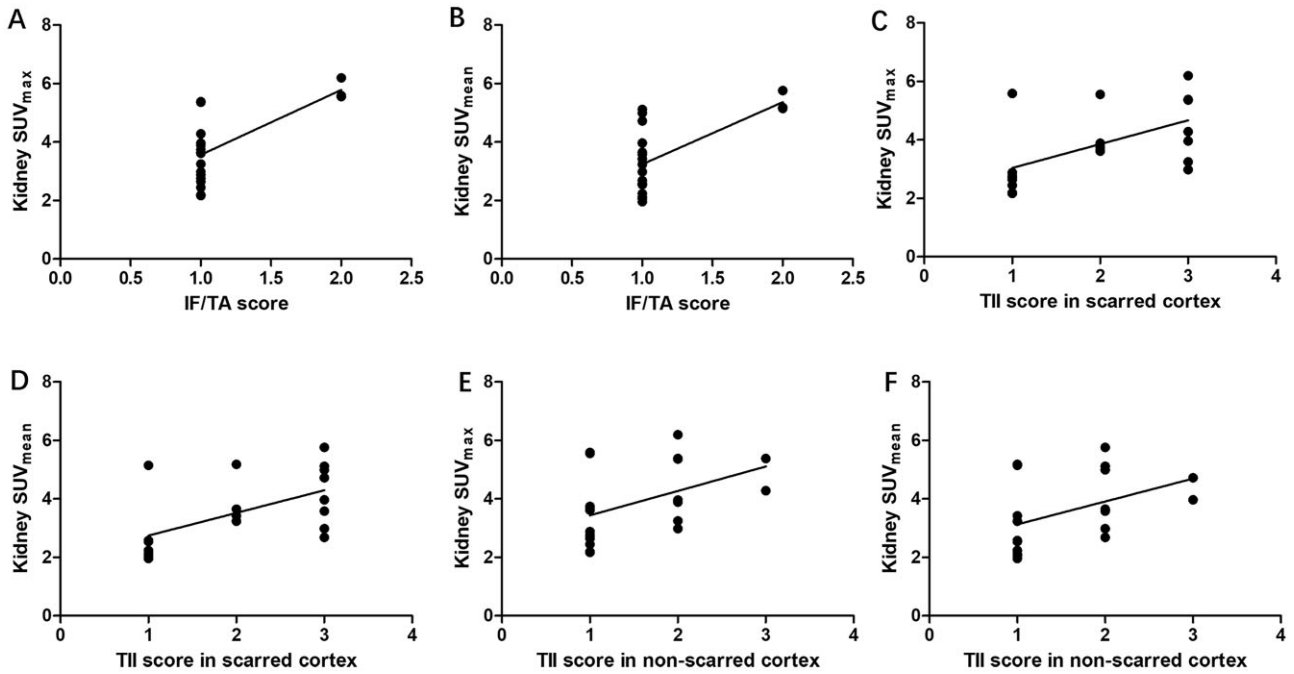

Figure 5: Correlation of the renal parenchymal FAPI uptake with renal inflammation and fibrosis scores. The SUV_{max} demonstrated a positive correlation with the IF/TA score ($r = 0.637$, $P = .003$) (**A**), and SUV_{mean} similarly showed a positive association with the IF/TA score ($r = 0.641$, $P = .002$) (**B**). SUV_{max} demonstrated a positive correlation with the TII score in scarred cortex ($r = 0.593$, $P = .006$) (**C**), and SUV_{mean} similarly showed a positive association with the TII score in scarred cortex ($r = 0.592$, $P = 0.006$) (**D**). A positive correlation was observed between SUV_{max} and SUV_{mean} with the TII score in non-scarred cortex ($r = 0.491$, 0.479, $P = .028$, $.033$) (**E**, **F**).

of [^{18}F]AlF-NOTA-FAPI-04 PET/CT scans in the timely evaluation of renal fibrosis in IgAN patients.

During the initial stage of the illness, the mesangial area is impacted by an inflammatory response, leading to the proliferation of mesangial cells and an anomalous production of the mesangial matrix. The inflammatory reaction impacts the capillary endothelial cells, podocytes and tubular cells [9]. Timely identification and proactive measures to address interstitial inflammatory cell infiltration can effectively decelerate the progression of interstitial fibrosis. Our research revealed a significant positive correlation between renal parenchymal FAPI uptake and TII score. Patients with high TII scores exhibited higher renal SUV_{max} and SUV_{mean} in both scarred and non-scarred cortex. Notably, the TII score in the scarred cortex was significantly higher than that in the non-scarred cortex. These results align with our previous study across different kidney disease types, suggesting that [^{18}F]AlF-NOTA-FAPI-04 PET/CT imaging holds promise for inflammation assessment in IgAN patients. This is crucial for early-stage IgA patients without evident pathological changes, enabling early diagnosis and improved monitoring of disease activity and treatment response.

Previous studies have been conducted on MEST-C scores of clinical indicators to diagnose IgAN or predict IgAN. A study conducted in Brazil [39] demonstrated that clinical indicators can predict the MEST-C scores of IgAN. Specifically, hypertension was found to increase the likelihood of M1 by 2.54 times and T2 by 5 times compared with T0. Moreover, for each unit increase in creatinine, the probability of E1 increased by 2.6 times and C by 2.8 times. Additionally, every unit increase in eGFR was associated with a 6% decrease in the probability of T2 compared with T0. Another study by Kirac *et al.* [40] revealed that various biomarkers including C-reactive protein, Alb, uric acid, C3, C4, IgG, IgA, IgM levels, white blood cell count, and 24h-UP could predict histopathological diagnosis in patients with glomerulonephritis. Furthermore, a Japanese cross-sectional study [41] highlighted that segmental glomerular sclerosis or adhesions (S) had the most significant impact on proteinuria in patients with IgAN, while eGFR, mean arterial pressure and serum uric acid levels were primarily linked to S lesions and the extent of lesions. The study by Lang *et al.* suggested that serum IgA/C3 ratio and glomerular C3 staining may be useful markers for the progression of IgAN in children [42]. This study demonstrated statistically significant differences in BUN, Scr, UA, eGFR, Hb, Alb and serum C3 among patients classified into different M groups according to the Oxford classification. Additionally, BUN, Scr, UA, eGFR, Alb, serum IgA and 24h-UP showed statistically significant differences in S groups. Among patients with varying T groups, UA, eGFR, Alb, serum IgA and 24h-UP also exhibited statistically significant differences. Conversely, among different E-group patients, statistical significance was observed only for Hb levels. In patients categorized by C group, statistical significance was noted solely in serum C4. These results suggest that patients exhibiting elevated BUN, Scr and UA, along with low eGFR and Alb levels, may experience severe mesangial cell hyperplasia, segmental glomerulosclerosis, and TA/IF. Furthermore, patients with increased IgA and 24h-UP may show a correlation with the extent of glomerulosclerosis and TA/IF. Additionally, low Hb levels were associated with exacerbated proliferation of mesangial and endothelial cells, while elevated C4 levels are more frequently observed in patients with crescentic disease. However, due to the small sample size, further confirmation is warranted through large-sample, multi-center studies.

Our study validated a strong negative relationship between FAPI uptake in the renal parenchyma and eGFR in individuals with IgAN. This finding aligned with our previous research on different types of kidney diseases. Additionally, Conen *et al.*

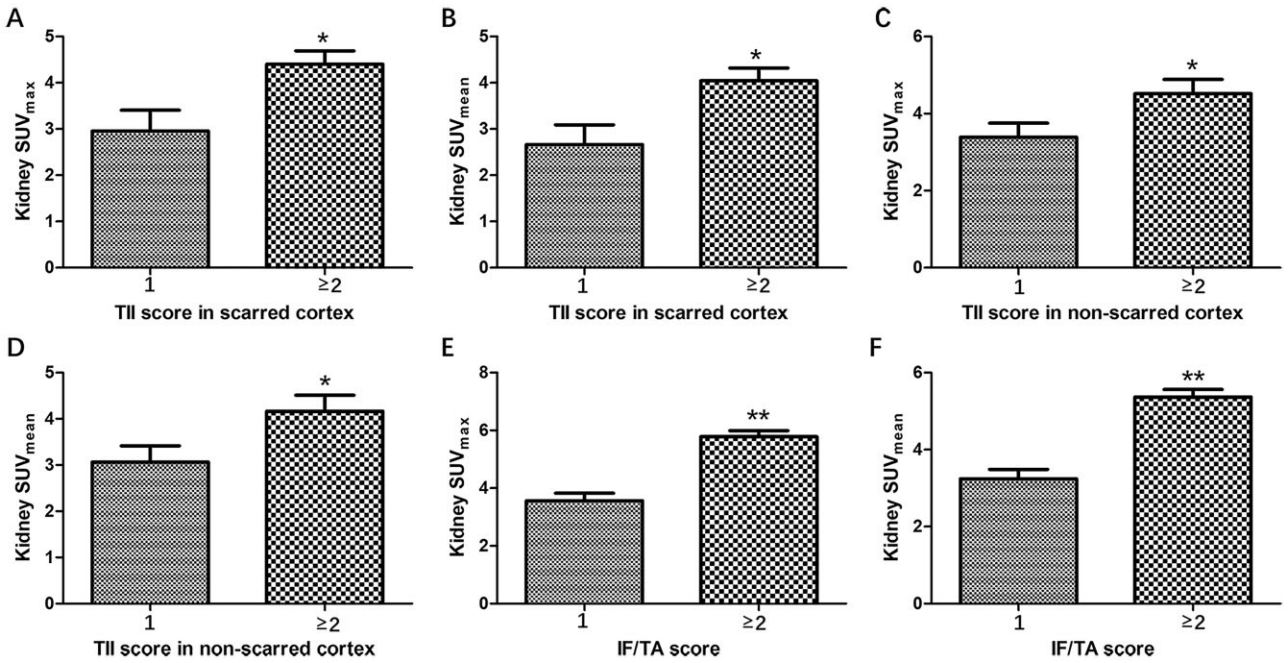

Figure 6: Comparison of the renal parenchymal FAPI uptake between patients with different severities of interstitial inflammation and fibrosis. (**A**, **B**) Individuals with mild renal interstitial inflammation in the scarred cortex (TII score = 1) exhibited significantly lower SUV_{max} and SUV_{mean} values compared with those with moderate to severe renal interstitial inflammation in the scarred cortex (TII score ≥2) (2.9 ± 1.2 vs 4.4 ± 1.0 and 2.7 ± 1.1 vs 4.0 ± 1.0, respectively; $t = -2.834$ and -2.831, both $P = .011$). (**C**, **D**) Patients with mild renal interstitial inflammation in the non-scarred cortex (TII score = 1) showed significantly lower SUV_{max} and SUV_{mean} values in relation to participants with moderate or severe renal interstitial inflammation in the non-scarred cortex (TII score ≥2) (3.4 ± 1.2 vs 4.5 ± 1.1 and 3.1 ± 1.1 vs 4.2 ± 1.0, respectively; $t = -2.157$ and -2.202, $P = .045$ and .041). (**E**, **F**) The assessment of interstitial fibrosis showed a similar pattern, with reduced levels of SUV_{max} and SUV_{mean} detected in individuals with mild interstitial fibrosis and tubular atrophy (IF/TA score = 1) compared with those with moderate or severe interstitial fibrosis and tubular atrophy (IF/TA score ≥2) (3.6 ± 1.1 vs 5.8 ± 0.4, 3.2 ± 1.0 vs 5.4 ± 0.3, respectively; $t = -3.509$ and -3.543, $P = .003$ and .002). $^{**}P < .01$, $^{*}P < .05$.

[28] observed a significant negative correlation between renal parenchymal ^{68}Ga-FAPI uptake and GFR, highlighting the potential of ^{68}Ga-FAPI for the noninvasive quantitative evaluation of kidney fibrosis. Furthermore, we identified a significant difference in renal parenchymal FAPI uptake among the various categories of the Oxford classification, particularly in patients exhibiting more severe mesangial cell hyperplasia, segmental glomerulosclerosis and TA/IF. These results suggest

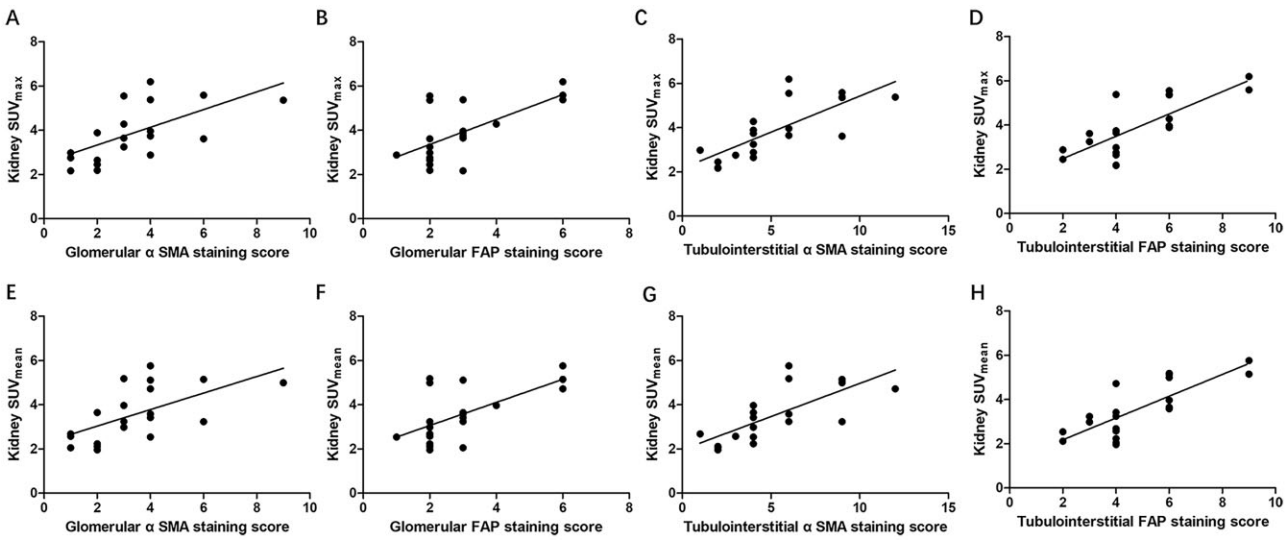

Figure 7: Correlation of the renal parenchymal FAPI uptake with immunohistochemical staining results. (**A**, **B**) The SUV_{max} showed a positive correlation with the staining score for glomerular αSMA and FAP ($r = 0.667$ and 0.604, both $P < .01$). (**C**, **D**) The SUV_{max} exhibited a positive correlation with the staining score for tubulointerstitial αSMA and FAP ($r = 0.781$ and 0.758, both $P < .001$). (**E**, **F**) The SUV_{mean} showed a positive correlation with the staining score for glomerular αSMA and FAP ($r = 0.622$ and 0.578, both $P < .01$). (**G**, **H**) The SUV_{mean} exhibited a positive correlation with the staining score for tubulointerstitial αSMA and FAP ($r = 0.755$ and 0.779, both $P < .001$).

that the level of renal FAPI uptake may serve as an indirect marker for eGFR and could aid in predicting the severity of nephropathy in IgAN.

This study has several limitations that should be acknowledged. Firstly, it is a single-center study with patients experiencing different disease courses, potentially leading to selection bias. Secondly, while this study preliminarily analyzed the relationship between each parameter of the patient's Oxford classification and various clinical indicators, as well as renal FAPI uptake, the limited sample size constrains the reliability of the results. Thirdly, ethical and medical cost constraints prevented patients from undergoing a second post-treatment PET/CT imaging, limiting the study's ability to evaluate the efficacy of IgAN treatment using [^{18}F]AlF-NOTA-FAPI-04 PET/CT. In future studies, we will optimize the patient inclusion criteria to minimize selection bias. Additionally, we will expand the sample size and conduct a multi-center study to further investigate the correlation between renal parenchymal FAPI uptake and various clinical indicators and pathological grades. This approach aims to provide more substantial evidence for the non-invasive monitoring of [^{18}F]AlF-NOTA-FAPI-04 PET/CT in patients with IgAN.

CONCLUSIONS

PET/CT imaging using [^{18}F]AlF-NOTA-FAPI-04 offers a non-invasive method for evaluating inflammation and fibrosis, potentially providing valuable insights into the pathological severity in IgAN patients. This imaging technique could significantly improve evaluation strategies for monitoring disease progression after the initial biopsy, thereby reducing the necessity for repeat biopsies.

SUPPLEMENTARY DATA

Supplementary data are available at *Clinical Kidney Journal* online.

FUNDING

This work was supported by Science and Technology Project of Sichuan Provincial Health Commission (23LCYJ023), Natural Science Foundation of China (81960320) and the Natural Science Foundation of Sichuan Province (2023NSFSC0635).

DATA AVAILABILITY STATEMENT

The data used to support the findings of this study are available from the corresponding author upon request.

CONFLICT OF INTEREST STATEMENT

The authors declare no conflict of interest.

REFERENCES

1. Hassler JR. IgA nephropathy: a brief review. *Semin Diagn Pathol* 2020;**37**:143–7. https://doi.org/10.1053/j.semdp.2020.03.001
2. Chang S, Li XK. The role of immune modulation in pathogenesis of IgA nephropathy. *Front Med (Lausanne)* 2020;**7**:92. https://doi.org/10.3389/fmed.2020.00092
3. Dotz V, Visconti A, Lomax-Browne HJ *et al.* O- and N-glycosylation of serum immunoglobulin A is associated with IgA nephropathy and glomerular function. *J Am Soc Nephrol* 2021;**32**:2455–65. https://doi.org/10.1681/ASN.2020081208
4. Habas E, Ali E, Farfar K *et al.* IgA nephropathy pathogenesis and therapy: review & updates. *Medicine (Baltimore)* 2022;**101**:e31219.
5. Ohyama Y, Renfrow MB, Novak J *et al.* Aberrantly glycosylated IgA1 in IgA nephropathy: what we know and what we don't know. *J Clin Med* 2021;**10**:3467. https://doi.org/10.3390/jcm10163467
6. Black LM, Lever JM, Agarwal A. Renal inflammation and fibrosis: a double-edged sword. *J Histochem Cytochem* 2019;**67**:663–81. https://doi.org/10.1369/0022155419852932
7. Meng XM. Inflammatory mediators and renal fibrosis. *Adv Exp Med Biol* 2019;**1165**:381–406. https://doi.org/10.1007/978-981-13-8871-2_18
8. Roberts IS. Oxford classification of immunoglobulin A nephropathy: an update. *Curr Opin Nephrol Hypertens* 2013;**22**:281–6. https://doi.org/10.1097/MNH.0b013e32835fe65c
9. Schena FP, Rossini M, Abbrescia DI *et al.* The molecular mechanisms of inflammation and scarring in the kidneys of immunoglobulin A nephropathy: gene involvement in the mechanisms of inflammation and scarring in kidney biopsy of IgAN patients. *Semin Immunopathol* 2021;**43**:691–705. https://doi.org/10.1007/s00281-021-00891-8
10. Li S, Hao H, Li R *et al.* Urinary exosomal MicroRNAs as new noninvasive biomarkers of IgA nephropathy. *Tohoku J Exp Med* 2022;**256**:215–23. https://doi.org/10.1620/tjem.256.215
11. Klinkhammer BM, Lammers T, Mottaghy FM *et al.* Non-invasive molecular imaging of kidney diseases. *Nat Rev Nephrol* 2021;**17**:688–703. https://doi.org/10.1038/s41581-021-00440-4
12. Luciano RL, Moeckel GW. Update on the native kidney biopsy: core curriculum 2019. *Am J Kidney Dis* 2019;**73**:404–15. https://doi.org/10.1053/j.ajkd.2018.10.011
13. Yavas H, Sahin OZ, Ersoy R *et al.* Prognostic value of NGAL staining in patients with IgA nephropathy. *Ren Fail* 2013;**35**:472–6. https://doi.org/10.3109/0886022X.2013.767114
14. Xu PC, Zhang JJ, Chen M *et al.* Urinary kidney injury molecule-1 in patients with IgA nephropathy is closely associated with disease severity. *Nephrol Dial Transplant* 2011;**26**:3229–36. https://doi.org/10.1093/ndt/gfr023
15. Mori K, Lee HT, Rapoport D *et al.* Endocytic delivery of lipocalin-siderophore-iron complex rescues the kidney from ischemia-reperfusion injury. *J Clin Invest* 2005;**115**:610–21. https://doi.org/10.1172/JCI23056
16. Navarro-Muñoz M, Ibernon M, Bonet J *et al.* Uromodulin and α(1)-antitrypsin urinary peptide analysis to differentiate glomerular kidney diseases. *Kidney Blood Press Res* 2012;**35**:314–25. https://doi.org/10.1159/000335383
17. Khatir DS, Pedersen M, Jespersen B *et al.* Reproducibility of MRI renal artery blood flow and BOLD measurements in patients with chronic kidney disease and healthy controls. *J Magn Reson Imaging* 2014;**40**:1091–8. https://doi.org/10.1002/jmri.24446
18. Liu Y, Zhang GM, Peng X *et al.* Diffusional kurtosis imaging in assessing renal function and pathology of IgA nephropathy: a preliminary clinical study. *Clin Radiol* 2018;**73**:818–26. https://doi.org/10.1016/j.crad.2018.05.012
19. Zhang L, Chen Z, Feng L *et al.* Preliminary study on the application of renal ultrasonography radiomics in the classification of glomerulopathy. *BMC Med Imaging* 2021;**21**:115. https://doi.org/10.1186/s12880-021-00647-8

20. Mao W, Ding X, Ding Y *et al*. Does bi-exponential fitting perform better than mono-exponential fitting in IVIM-DWI? An assessment of renal pathological injury of IgA nephropathy. *Curr Med Imaging* 2023;**20**. https://doi.org/10.2174/1573405620666230627103919
21. Levy MT, McCaughan GW, Abbott CA *et al*. Fibroblast activation protein: a cell surface dipeptidyl peptidase and gelatinase expressed by stellate cells at the tissue remodelling interface in human cirrhosis. *Hepatology* 1999;**29**:1768–78. https://doi.org/10.1002/hep.510290631
22. Dendl K, Koerber SA, Kratochwil C *et al*. FAP and FAPI-PET/CT in malignant and non-malignant diseases: a perfect symbiosis. *Cancers (Basel)* 2021;**13**:4946. https://doi.org/10.3390/cancers13194946
23. Kratochwil C, Flechsig P, Lindner T *et al*. (68)Ga-FAPI PET/CT: tracer uptake in 28 different kinds of cancer. *J Nucl Med* 2019;**60**:801–5. https://doi.org/10.2967/jnumed.119.227967
24. Fitzgerald AA, Weiner LM. The role of fibroblast activation protein in health and malignancy. *Cancer Metastasis Rev* 2020;**39**:783–803. https://doi.org/10.1007/s10555-020-09909-3
25. Rosenkrans ZT, Massey CF, Bernau K *et al*. [(68) Ga]Ga-FAPI-46 PET for non-invasive detection of pulmonary fibrosis disease activity. *Eur J Nucl Med Mol Imaging* 2022;**49**:3705–16. https://doi.org/10.1007/s00259-022-05814-9
26. Mao H, Chen L, Wu W *et al*. Noninvasive assessment of renal fibrosis of chronic kidney disease in rats by [(68)Ga]Ga-FAPI-04 small animal PET/CT and biomarkers. *Mol Pharm* 2023;**20**:2714–25. https://doi.org/10.1021/acs.molpharmaceut.3c00163
27. Zhou Y, Yang X, Liu H *et al*. Value of [^{68}Ga]Ga-FAPI-04 imaging in the diagnosis of renal fibrosis. *Eur J Nucl Med Mol Imaging* 2021;**48**:3493–501. https://doi.org/10.1007/s00259-021-05343-x
28. Conen P, Pennetta F, Dendl K *et al*. [^{68}Ga]Ga-FAPI uptake correlates with the state of chronic kidney disease. *Eur J Nucl Med Mol Imaging* 2022;**49**:3365–72. https://doi.org/10.1007/s00259-021-05660-1
29. Wang H, Zhang P, Wang W *et al*. [^{18}F] AlF-NOTA-FAPI-04 PET/CT for non-invasive assessment of tubular injury in kidney diseases. *Clin Kidney J* 2024;**17**:sfae064. https://doi.org/10.1093/ckj/sfae064
30. Levey AS, Stevens LA, Schmid CH *et al*. A new equation to estimate glomerular filtration rate. *Ann Intern Med* 2009;**150**:604–12. https://doi.org/10.7326/0003-4819-150-9-200905050-00006
31. Jiang X, Wang X, Shen T *et al*. FAPI-04 PET/CT using [^{18}F]AlF labeling strategy: automatic synthesis, quality control, and in vivo assessment in patient. *Front Oncol* 2021;**11**:649148. https://doi.org/10.3389/fonc.2021.649148
32. Trimarchi H, Barratt J, Cattran DC *et al*. Oxford Classification of IgA nephropathy 2016: an update from the IgA Nephropathy Classification Working Group. *Kidney Int* 2017;**91**:1014–21. https://doi.org/10.1016/j.kint.2017.02.003
33. Gomes MF, Mardones C, Xipell M *et al*. The extent of tubulointerstitial inflammation is an independent predictor of renal survival in lupus nephritis. *J Nephrol* 2021;**34**:1897–905. https://doi.org/10.1007/s40620-021-01007-z
34. Yeter HH, Gonul I, Guz G *et al*. Combining clinical features and MEST-C score in IgA nephropathy may be a better determinant of kidney survival. *Rom J Intern Med* 2020;**58**:209–18.
35. Cattran DC, Coppo R, Cook HT *et al*. The Oxford classification of IgA nephropathy: rationale, clinicopathological correlations, and classification. *Kidney Int* 2009;**76**:534–45. https://doi.org/10.1038/ki.2009.243
36. Feldmann Y, Böer K, Wolf G *et al*. Complications and monitoring of percutaneous renal biopsy—a retrospective study. *Clin Nephrol* 2018;**89**:260–8. https://doi.org/10.5414/CN109223
37. Rockey DC, Bell PD, Hill JA. Fibrosis—a common pathway to organ injury and failure. *N Engl J Med* 2015;**373**:96.
38. Rajasekaran A, Julian BA, Rizk DV. IgA nephropathy: an interesting autoimmune kidney disease. *Am J Med Sci* 2021;**361**:176–94. https://doi.org/10.1016/j.amjms.2020.10.003
39. Monteiro M, Vieira MR, Pereira L *et al*. Is it possible to predict parameters of the Oxford classification of primary IgA nephropathy from clinical laboratory data? Focus on the role of segmental glomerulosclerosis subtypes. *Pathol Res Pract* 2019;**215**:152533. https://doi.org/10.1016/j.prp.2019.152533
40. Kirac Y, Bilen S, Duranay M. Comparison of laboratory findings in patients with glomerulonephritis classified according to histopathologic diagnosis. *Minerva Med* 2014;**105**:149–56.
41. Kamano C, Shimizu A, Joh K *et al*. A cross-sectional study in patients with IgA nephropathy of correlations between clinical data and pathological findings at the time of renal biopsy: a Japanese prospective cohort study. *Clin Exp Nephrol* 2021;**25**:509–21. https://doi.org/10.1007/s10157-021-02022-x
42. Lang Y, Song S, Zhao L *et al*. Serum IgA/C3 ratio and glomerular C3 staining predict progression of IgA nephropathy in children. *Transl Pediatr* 2021;**10**:666–72. https://doi.org/10.21037/tp-21-90

Received: 9.6.2024; Editorial decision: 30.9.2024